

Simulation Prediction and Flight Validation of UH-60A Black Hawk Slung-Load Characteristics

Peter H. Tyson
Naval Postgraduate School, Monterey, CA

Luigi S. Cicolani
Army/NASA Rotorcraft Division, Ames Research Center, Moffett Field, CA

Mark B. Tischler
Army/NASA Rotorcraft Division,
Aeroflightdynamics Directorate, U.S. Army Aviation and Missile Command,
Ames Research Center, Moffett Field, CA

Aviv Rosen and Daniel Levine
Dept. of Aerospace Engineering, Technion Institute of Technology, Haifa, Israel

Munro Dearing
Army/NASA Rotorcraft Division, Ames Research Center, Moffett Field, CA

Abstract

This paper describes the development and validation of a slung-load simulation model obtained by integrating the GenHel blade-element and components-type simulation of the UH-60A with the slung-load equations of motion. The load aerodynamics model accounts for rotor downwash effects and static aerodynamics. The downwash model is based on momentum theory and empirical wake velocity data. Static aerodynamics for the CONEX cargo container were obtained from wind tunnel tests. The simulation validation is based primarily on comparison with flight test frequency response data. Frequency sweep flight test data, including load motion data, have been obtained at Ames in recent years for test loads which included an aerodynamically inert steel block and the aerodynamically active CONEX. It is shown that the simulation, validated for on-axis response dynamics over the frequency range of interest in handling qualities, [0.05, 2] Hz, can predict some of the key handling qualities and system stability parameters of interest in evaluating and certifying helicopter slung-load configurations.

Introduction

Helicopter slung-load operations are common in both military and civil contexts. Helicopter slung-load configurations are two-body dynamic systems in which the load adds its rigid body dynamics, aerodynamics, and sling stretching dynamics to that of the helicopter. The slung load can degrade the handling qualities of the helicopter and reduce the flight envelope of the combined system below that of the helicopter alone. Further, the effects of the load vary significantly among the load-sling combinations that a utility helicopter will encounter during its operational life. External load accidents accounted for about 11% of all civil helicopter accidents over a recent 7 year period, and these accidents are often deadlier than other kinds of helicopter mishaps.^{1,2} Therefore, confirmation of the system stability, handling qualities and operating envelope is desired. Currently, qualitative flight evaluations are done to certify particular external load configurations for military operational transport.³ Sometimes extensive flight programs and tests are performed to certify load carrying capacity,⁴ but these are time consuming, and it can be prohibitively costly to test the entire operating range of slung-load configurations.

Presented at the AHS 55th Annual Forum, Montreal, Canada, May 25–27, 1999. Copyright © 1999 by the American Helicopter Society, Inc. All rights reserved.

A simulation model validated over the range of frequencies of interest in handling qualities assessments would significantly reduce the costs associated with slung-load evaluations by allowing realistic analytical evaluation for

load clearance and prediction of critical flight conditions, development of handling qualities requirements for slung loads, parametric studies and configuration optimization, and load stabilization studies.

In this context, an exploratory project was initiated at Ames in which flight tests were conducted to demonstrate an efficient method for obtaining analytical results at flight time^{5,6}; to accumulate a database of flight data with the UH-60A as the test aircraft; and to develop and validate a simulation model.

The paper begins with a description of the data available for the validation from previous slung-load flight tests at Ames, followed by a discussion of the key dynamic parameters of interest for slung-load evaluations and a description of the simulation model. Finally, validation methods and results are given. The database was obtained with a UH-60A helicopter carrying several loads, including the CONEX (CONtainer EXpress) cargo container, whose motions are strongly influenced by its aerodynamics, and loads with negligible aerodynamics; and these loads were suspended with a standard four-cable military sling about 16 ft long.⁵ The database consists principally of longitudinal and lateral axis frequency sweeps, since these are the axes most affected by the load in the frequency range of interest, [0.05, 2] Hz. The dynamic parameters of interest are handling qualities parameters, stability margins, and load pendulum stability. The helicopter model used in the simulation is the Sikorsky GenHel (Generalized Helicopter Simulation) blade-element model of the UH-60,⁷ which has previously been used and validated at Ames⁸⁻¹⁰ for handling qualities studies, and extensively validated at Sikorsky.⁴ This model is combined with the two-body slung-load equations of motion, a model of the rotor downwash field in the vicinity of the load, and load static aerodynamic data to complete the simulation. The validation is concerned principally with on-axis responses to control inputs over the frequency range of interest. The validation begins with an assessment of the GenHel model, then considers a configuration with the aerodynamically inert block load, and finally the CONEX load.

The slung-load program at Ames has been conducted under the NASA SAFOR program for flight safety and as part of a U.S. Army/Israel memorandum of agreement for cooperative research on rotorcraft aeromechanics and man-machine integration technology.¹¹ Under this agreement the United States has provided the aircraft, load, and test range, while Israel has provided the load instrumentation and wind tunnel testing.

Slung-Load Flight Test Database

Flight tests with a UH-60A helicopter and several test loads have been carried out periodically at Ames since 1995. Early tests focused on procedure checkout and familiarization with solid steel test loads having negligible aerodynamics. During 1997, tests focused on an instrumented $8 \times 6 \times 6$ ft CONEX container. Current flight tests are aimed at collecting data with an instrumented 4K lb steel block load. Flight data from these activities have been accumulated in a database. Details of the test configurations and instrumentation and a summary of the database (test flights, test loads, test points, and the measured and derived quantities) are given in Ref. 5.

Test Aircraft

The test aircraft is a sixth year production UH-60A Black Hawk utility helicopter. A cargo hook is mounted in the floor of the aircraft and gimballed in roll. The research Aircraft Data Acquisition System (ADAS) was installed during the airloads program,¹² and comprises several racks of dynamics sensors (accelerometers, rate and attitude gyros), telemetry equipment, and flight recorder mounted in the cabin; plus control system sensors (cockpit controls, mixers, primary servos, and feedback servos), air data sensors mounted on a nose boom, a low airspeed air data system, and a cargo hook strain gage.⁵ Some parameters of interest for the test aircraft are noted in Fig. 1 for later reference. Additional information on aircraft parameters can be found in Ref. 13.

Test Load-Sling Configurations

Data for the validation study come from the two test loads illustrated in Fig. 1. The sling is a standard four-legged military sling rated at 10K lb capacity. One load is a 4K lb steel block with the instrumentation package mounted on the top surface and a magnetic compass mounted on an aluminum boom extending from the rear of the block. This is a high-density test load with negligible specific aerodynamic forces and moments over the power-limited speed range of the helicopter. Load aerodynamics are not a factor in driving the motions of this load. The second load is a CONEX cargo container, which possesses significant aerodynamics, even in hover where rotor downwash results in a steady yaw rotation of 30–40 deg/sec if the sling is swiveled. It is limited to 60 kt in military operations,³ well below the 120 kt limit for UH-60 slung-load operations.

The load instrumentation is mostly contained in a single portable package mounted inside the CONEX on a rail at midheight or on top of the 4K block, plus a

boom-mounted fluxgate compass. The load sensors include linear accelerometers, rate gyros, and the magnetic compass. Parameter values for the sling and loads are included in Fig. 1. The principal load dynamics affecting aircraft stability margins and handling qualities are the load pendulum modes. Pendulum frequencies are determined by the load relative mass and sling length which can be estimated as $\sqrt{g/L(1+m_2/m_1)}$ where L is in the range 15–20 ft, m_2/m_1 is about 27%, and the pendulum frequencies are near 1.6 rad/sec for the test configurations. The hook-offset below the helicopter center of gravity (c.g.) (4.3 ft for the UH-60) couples the load motions with the helicopter attitude dynamics. The amount of specific moment from the hook force depends inversely on the helicopter inertia so that coupling effects are significantly greater for the lateral axis than for the longitudinal axis.

Flight Test Data

The present validation study uses data for the configurations and test airspeeds noted in Table 1. Tests with no load provide baseline data for validation of the helicopter model. The validation will focus on the longitudinal and lateral axes since the load primarily affects system dynamic characteristics for these axes in the frequency range of interest for handling qualities. The test data comprise pilot-generated frequency sweeps, principally for the longitudinal and lateral axes, plus step and doublet responses for all axes. A sample lateral axis sweep is shown in Fig. 2. Input frequency is varied smoothly over the range [0.05, 2] Hz, using reduced amplitude at low frequencies to avoid excess attitude excursions, and being careful to end the sweep at 2 Hz to avoid resonance with the lowest frequency, lightly damped rotor mode. Otherwise, the pilot uses occasional low amplitude, low

frequency off-axis inputs to maintain the aircraft centered about the reference trim condition. The aircraft roll rate responds at all frequencies, while load roll rate responds only for inputs near the pendulum frequency. More information on rotorcraft frequency sweep testing procedures and safety precautions is given in Ref. 14.

Flight Dynamic Characteristics

The dynamic parameters to be identified from flight data and predicted from simulation data provide an evaluation of the helicopter slung-load handling qualities and stability. These are the aircraft handling qualities parameters (bandwidth and phase delay), the aircraft stability margins (phase and gain margins), and the load pendulum roots (damping and natural frequency). These can be identified from frequency domain analysis of the frequency sweep data as described next, and their identification depends on the on-axis responses out to frequencies of 2+ Hz. The frequency domain analyses are carried out using the CIPHER® (Comprehensive Identification from Frequency Responses) software for interactive frequency domain analysis developed by the Army group at Ames.^{15,16} CIPHER® uses Chirp-Z fast Fourier transforms and can combine responses computed for several window sizes to optimize accuracy of the frequency responses at all frequencies. The flight data are available at 100 Hz, well above that needed to identify dynamics out to 2–3 Hz. Frequency responses are generated as the first harmonic approximation of the system dynamics from the time history data. The quality of this approximation is measured by the linear correlation between the identified response and the data at each frequency (coherence function), and should be above 0.6 for a credible result.

Table 1 Flight Test Matrix

Load	Airspeed (kt)					
	Hover	30	50	60	70	80
No load	X	X	X			X
4K lb block	X	X	X			X
4K lb CONEX	X	X	X	X	X	

Note: Instrumentation package not installed for the 4K block 80 kt test case

Handling Qualities Parameters

The handling qualities parameters are computed as illustrated in Fig. 3 from the Bode plot of the aircraft attitude response with a load. For feedback systems with rate command response, such as the UH-60 system, bandwidth is the smaller of the two frequencies corresponding to 45 deg phase margin and 6 dB gain margin from instability. Phase delay is proportional to the rate at which phase changes at the 180 deg phase shift frequency. It reflects how fast the coupled pilot-vehicle system loses stability at this frequency. Larger values imply a more rapid loss of stability and result in pilot complaints about tendencies toward pilot-induced oscillations. The corresponding handling qualities are rated as satisfactory if the combination of bandwidth and phase delay is within the region labeled Level 1 in Fig. 3. Other regions are Level 2 (satisfactory with improvement) and Level 3 (unsatisfactory). The regions shown are established in the Army's Aeronautical Design Standard, ADS-33 (Ref. 17) based on data for scout attack helicopters. Corresponding boundaries for utility helicopters and for slung-load operations have not yet been defined but are under study by the Army. The ADS-33 boundaries are used tentatively to predict handling qualities ratings for slung loads in the present work. The effects of the load on the frequency response are seen as a gain dip and phase shift near the pendulum frequency. These effects increase with load weight.

Stability Margins

The computation of stability margins is illustrated in Fig. 4. These margins are computed from the feedback loop response of the SAS (Stability Augmentation System) servo output to the total control signal and are defined only for those axes with active feedback loops. Phase margin (PM) is defined at the crossover frequency and gain margin is defined at the frequency for 180 deg phase shift. Multiple crossovers can occur, as in the Fig. 4, in which case phase margin is taken as the smallest margin for crossings in the frequency range of interest. In some cases there are no crossings, and in those cases the system can never be driven unstable and the phase margin is considered infinite. The plot shows gain margin (GM) at the lowest frequency with 180 deg phase shift, which is associated with the rotor-airframe rigid body degrees of freedom. Higher such frequencies occur in association with fuselage bending modes, and these can be the critical gain margins for flexible aircraft, such as the CH-53E (Ref. 4) or MH-53J (Ref. 18). However, the UH60 airframe is comparatively stiff so that the lowest frequency gain margin is considered to be the most important and will be critical for determining closed-loop

response characteristics. In any case, the present scope of study is limited to 2+ Hz and below. Typical military requirements for stability margins are 6 dB gain margin and 45 deg phase margin. The effect of the load on the control loop frequency response appears as a gain dip and phase shift near the pendulum frequency.

Pendulum Roots

The load adds a number of modes to those of the helicopter alone. Of these, only the pendulum modes interact with the helicopter in the frequency range of interest. Simulation analysis indicates that the pendulum modes at hover are decoupled longitudinal and lateral pendulum motions relative to the helicopter, and that these motions are readily excited by lateral and longitudinal control inputs. Consequently, the load pendulum roots can be identified from the load on-axis angular rate response as shown in Fig. 5. The response is seen to have a gain peak and 180 deg phase shift in the neighborhood of the pendulum frequency (about 1.6 rad/sec for the test loads) which reflects the presence of a second-order pole that can be identified by fitting the response in the vicinity of the pendulum frequency. This is performed with CIPHER®'s NAVFIT utility, over a range of one half to twice the pendulum frequency. A cost function, which is a weighted combination of the squares of the gain and phase fitting errors, measures the accuracy of the hypothesized model, and should be below 100 for the model to be a good approximation. In general, the load can rotate in yaw relative to the helicopter, so that it is necessary to transform the measured load pitch and roll rates to a frame aligned with the helicopter longitudinal and lateral axes for the identification.

Slung-Load Simulation

The slung-load configurations of interest for this paper are helicopters carrying a load attached at a single point by multi-cable suspensions. More generally, operational and proposed slung-load configurations can include two or more suspension points, two or more loads, two or more helicopters, and various sling or suspension arrangements. A general approach to formulating the rigid body equations of motion (EOMs) for this class of multi-body systems is given in Refs. 19 and 20 along with the EOMs for several generic configurations, including the configuration of interest in this paper.

In aeronautical laboratories such as Ames, aircraft simulations are normally available with a standardized implementation of the Newton-Euler rigid body EOMs. Slung loads can be appended to such simulations using

the structure shown in Fig. 6. The load aerodynamics and multi-body EOMs are appended as shown and used to compute the hook forces and c.g. moments which are then added to the aircraft force and moment sums to drive its single rigid body dynamics. The two-body dynamics module necessarily carries a duplicate copy of the aircraft Newton-Euler equations. The two sets of aircraft states are coordinated by resetting the helicopter position and velocity states in the multi-body equations to those in the aircraft equations at the start of each computation cycle.

This arrangement has been used in slung-load simulations at Ames. In the present study, the load aerodynamics and two-body EOM modules were appended to an existing UH-60 simulation based on Sikorsky's GenHel model. The load-sling modules include load static aerodynamics and downwash effects, and the sling can be elastic or inelastic. In other work at Ames, a moving-base simulation has been implemented with single- and multi-cable suspensions, and two-point suspensions. The multi-cable model from that simulation was integrated into the GenHel UH-60 simulation for the present study. The integration was facilitated by the standardized modularization and interfaces for simulations at the Ames simulation lab.

GenHel Rotor/Helicopter Model

The GenHel nonlinear mathematical model of the UH-60A Black Hawk helicopter was developed by Sikorsky Aircraft⁷ to provide an engineering simulation suitable for performance and handling qualities evaluation. GenHel has been implemented at Ames in both real time and non-real time environments and has been validated at Ames both analytically and in a moving-base piloted simulation.⁸⁻¹⁰ It therefore provides a good starting point for the present work focused on validating the slung-load portion of the simulation.

The major components of GenHel are depicted in Fig. 7 (after Ref. 9). The airframe is represented as a rigid body. The main rotor model represents each blade as a rigid body, and includes flap-lag degrees of freedom for each blade plus air mass and hub rotational degrees of freedom. Blade-element theory is used for the main rotor; each blade is divided into five elements and the total blade forces and moments are computed as summations of the aerodynamic, inertial, and weight forces on the elements. Inflow is computed from the Pitt/Peters dynamic inflow model.²¹ The UH-60A engines are represented by a thermodynamic-cycle components model of the T700 engine and drive train.²² Linearized Bailey theory²³ is used for the tail rotor thrust computation. The model accounts for rotor downwash effects on the fuselage, empennage,

and tail rotor using tables based on wind tunnel data. The flight control system model mirrors the physical elements of the UH-60A flight control system, and this allows the GenHel control system outputs to correspond directly to quantities measured on the aircraft.

Slung-Load Equations of Motion

The two-body equations of motion for general multi-cable slings suspended from a single point were implemented as given in App. B of Ref. 17. The generic configuration is shown in Fig. 8 and represents slings with three or more legs attached at lift points on the load such that at least three sling leg directions are independent. The bodies are assumed rigid bodies and the sling legs can be elastic or inelastic. The hook-sling attachment is modeled as one which can transmit forces but not moments.

The parameters required for these equations are the masses and inertia matrices of the two bodies, the helicopter-c.g.-to-hook coordinates, the load-c.g.-to-lift-point coordinates, and the unloaded cable lengths and cable stretching parameters. Parameter values for the test configurations are listed in Fig. 1.

Sling stretching is conventionally modeled as a lightly damped spring which supports only tension. Parameter values for this model were identified in dynamic tests. However, it was found in moving-base piloted simulation studies at Ames that the elastic cable model results in excessive hook force excursions applied to the aircraft and sensed by the pilot, and is unrealistic. Consequently, only the inelastic cable dynamics will be considered in the validation. This suffices for present purposes since cable stretching dynamics have not been observed in the frequency range of this study. However, they have been implicated in incidents involving vertical bounce dynamics and would be essential in the study of higher frequency load-airframe-rotor interactions.

Simulations of isolated helicopters are normally initialized in static equilibrium using a gradient search computational procedure. The load-sling combination is readily integrated into this scheme by computing the hook force at each iteration from the force and moment balance equations of the load-sling subsystem. For inelastic slings, load moment balance is used to compute load attitude after which the inertial components of the hook force can be computed from load force balance. Variations in load aerodynamics with attitude are treated by iteration of small nonlinear terms in the load-sling equations starting from an initial attitude estimate. If the sling is elastic, then the effects of stretching on load attitude are included in the iteration. The effects of downwash on load aerodynamics

are included in the “outer loop” iteration of the helicopter equations.

Main Rotor Wake Model

The rotor downwash results in a significant airflow over the load in hover, on the order of 50 kt. Consequently a wake model was included in the simulation. Wake geometry is illustrated in Fig. 9 (after Ref. 24). The inflow air flows downward perpendicular to the tip path plane. Velocity varies from the inflow velocity at the rotor to twice that in the far-field where the wake cross section has contracted to half the rotor disk area. The far-field wake is fully developed at a distance of about 1.5 radii from the rotor. This velocity field, combined with the forward or sideward velocity of the aircraft, determines the locus of the wake centerline in space. The distribution of axial velocity in the wake is defined from measurements given in Ref. 25 as a function of distance below the rotor and radial distance from the center of the wake. Tangential wake velocity is computed from an empirical relation between axial and tangential flow given in Ref. 26. The air velocity at the load is computed according to the location of the load c.g. in the wake.

Load Static Aerodynamic Forces and Moments

The available measurements of load aerodynamics come principally from studies of the $8 \times 8 \times 20$ ft MILVAN cargo container and a few other loads made in the early 1970s in support of the heavy lift helicopter development (e.g., Refs. 27–31). Currently, wind tunnel studies have been conducted on the HUMVEE vehicle in support of V-22 Osprey development³² and on the CONEX for this project. Wind tunnel measurements have usually been limited to the load’s static aerodynamics (steady state variations with air velocity direction), and to studies of the critical airspeed at which an aerodynamically active load becomes unstable. A comprehensive model structure is not available for loads generally nor for any single load, but is expected to include the effects of load angular rates and unsteady aerodynamic phenomena, as well as the static aerodynamics.

The CONEX has been observed in the current flight tests to adopt a steady trail angle in proportion to drag (as do all loads). The CONEX also exhibits significant yaw rates which can be as much as 45 deg/sec in hover due to swirl in the rotor downwash, and which increase past 100 deg/sec for speeds above 50 kt. These yaw rates are steady if a swivel is used, and periodic with sling wind-up and unwinding if no swivel is used. Thus far, only static aerodynamics have been measured and these are presented here.

Drag-Only Aerodynamics. The simulation includes options for drag-only load aerodynamics and the CONEX static aerodynamics. In the drag-only estimation, load drag is represented by the parameter, D/q , independent of airspeed. The body-axes aerodynamics are:

$$\mathbf{FA2}_2 = -(D/q) 0.5 \rho \mathbf{V}a2 (u_2, v_2, w_2)$$

$$\mathbf{MA2}_2 = (0, 0, 0)$$

where $\mathbf{FA2}$, $\mathbf{MA2}$ are the load aerodynamic force and c.g. moment vectors, $\mathbf{V}a2$ is the airspeed at the load c.g., and (u_2, v_2, w_2) are the load body axes air velocity components. For many loads a single value of D/q independent of velocity direction suffices. For the CONEX load, the value of D/q varies from 42 to 88 ft² depending on direction. Drag for the more elongated MILVAN varies from 60 to 210 ft² depending on orientation.

CONEX Static Aerodynamics Wind Tunnel Testing. Wind tunnel tests were conducted at the Technion in Israel to measure the static aerodynamics of the CONEX. A 5.7% scale model (Fig. 10a) was manufactured ($5.8 \times 4.5 \times 4.5$ in), including the corrugations of the CONEX wall and the skids. The model was mounted on a sting balance that measures all six aerodynamic force and moment components. Inside the model there is a mechanism to change the pitch and roll angles over a range of ± 25 deg relative to the balance.

The tests were carried out at the Technion’s open-circuit fan-driven low-speed wind tunnel, which has a $1 \text{ m} \times 1 \text{ m} \times 3 \text{ m}$ long test section and can reach speeds of 58 kt (Fig. 10b). The tunnel has good uniformity of flow within 1% over the cross section except very near the tunnel walls. There are various mechanisms for mounting the model and sting. For the CONEX tests, the model and sting were mounted on the “banana” arm (Fig. 10c) which is, in part, a circular arch and connected in the middle of the floor to a rotating plate which can rotate through 360 deg, and to a bearing in the ceiling. The sting balance is connected to an extension arm attached to the arch and the extension arm can be positioned in intervals of 2.5 deg around the arch from vertical to 10 deg above the horizontal. This arrangement maintains the model in the center of the tunnel cross section. The possible arrangements of model and extension arm allow a range in model pitch over $[-115, 25]$ deg and a 360 deg range of yaw.

The tests were conducted at 39 kt tunnel speed. Tests at several flow speeds indicated negligible variations of the coefficients with tunnel speed. Runs were done by rotating the banana arm over ± 180 deg in yaw about the tunnel

centerline at 2.5 deg/sec with fixed model angles relative to the sting and fixed mounting angle of the extension arm on the banana arm. During the rotation, measurements of the flow speed, arch angle relative to the flow, and the six aerodynamic components were made at 5 KHz, normally averaging the data over 0.1 sec intervals (yaw intervals of 0.25 deg). Each run included more than 700 points, and more than 30 runs were made for the CONEX data. Wind axes results were computed for grids of α , β every 5 deg. The α , β values for each measurement point were computed and the measurements assigned to "bins" corresponding to each of the grid points. Statistics were computed for each bin, and symmetry rules could be applied between appropriate bins.

Simulation Static Aerodynamic Model. Tables of the static aerodynamic parameters were derived from the tunnel measurements for the angle of attack (AOA) and sideslip domain $\alpha \times \beta = [-90, 90] \times [0, 90]$ deg. Extension to negative sideslip uses symmetry properties (drag and lift are symmetric, side force and yaw moment are antisymmetric). Small modifications of the tunnel data were made to impose some symmetry properties; that is, side force and yaw moments pass through zero at $\beta = [0, 90]$ deg and drag is fixed for $\beta = 90$ deg. An apparent fixed bias was removed from the lift function. No modifications were made to impose expected symmetries in AOA about 0 deg pending further tests for systematic tunnel errors. Tunnel measurements were not made for $\alpha > 30$ deg and excursions above 30 deg are unlikely in flight. Nevertheless, the data were extended into this region by linear extrapolation for the simulation model. The results are shown in Fig. 11 where the aerodynamics are plotted versus sideslip (or AOA) for fixed values of AOA (or sideslip) every 10 deg. Drag is the largest force; it reaches a minimum at 90 deg sideslip where the CONEX has the minimum frontal area and looks identical to the axial flow independent of pitch, and it tends to increase with AOA owing to the skids on the bottom of the CONEX, which trap air. Side force is positive at all positive sideslip with similar variations versus sideslip for all AOA. For small sideslip angles, lift is approximately antisymmetric in AOA about zero and reaches peak values at about 15 deg. This behavior is repeated in the vicinity of $\alpha = -90$ deg. At sideslip angles above 20 deg, lift is small everywhere. Yaw moment has similar behavior at all AOA and is statically stable at $\beta = [0, 90]$ deg.

Simulation Validation and Prediction

Validation is based on a comparison of simulation and flight-generated frequency responses required to compute

the key dynamic parameters of interest, and on a comparison of the parameter values obtained. The comparison considers the on-axis responses over the frequency range of interest in handling qualities work. The discussion will consider, in order, the helicopter alone, the 4K lb block load, and the CONEX load.

Simulation data were obtained via computer-generated frequency sweeps. The simulation aircraft was maintained centered about the reference flight condition by adding a three-channel low gain rate and attitude feedback loop (following Ref. 33). The effects of correlated off-axis control inputs on the on-axis frequency responses due to the stabilizing control were removed using CIFER®'s MISOSA routine for multi-input, single-output analysis.

The aircraft simulation-flight match can be evaluated using the proposed FAA level D simulation certification criteria for flight training simulators with acceptable reproduction of aircraft handling qualities.¹⁶ An error function is formed by dividing the simulation attitude response by the flight response. Identical responses would produce unity (0 dB gain and 0 deg phase). The proposed criteria provide envelope boundaries for the error gain and phase within which the actual error function must fall for satisfactory reproduction of handling qualities. These boundaries vary with frequency over the range of [0, 20] rad/sec as can be seen in the lower part of Fig. 12. Excursions of the error function outside these boundaries indicate frequency ranges where the simulation falls short of the required fidelity. The error function can then be fitted with a low-order transfer function to obtain an empirical correction to tune the simulation at one or more flight conditions.

No-Load Simulation Fidelity

Handling Qualities Parameters. The GenHel and flight attitude responses and the error functions are shown in Fig. 12 for hover for longitudinal and lateral axes. The results show that the lateral axis error function magnitude is within the boundaries but phase is outside the boundary above 8 rad/sec, while the longitudinal axis gain and phase are both outside the boundary at higher frequencies. Thus, GenHel cannot adequately reproduce the frequency response in the region of 2 Hz where the phase shift reaches 180 deg. This region is crucial in determining handling qualities parameters. Note that the GenHel's phase shift drops more slowly than the flight data in this region, and thus GenHel will yield optimistic results.

The error functions were fitted with a simple gain and time delay. This exercise was repeated at all test airspeeds and average time delays of [48.5, 51.0] msec were

computed for the lateral and longitudinal axes, respectively, and a gain correction factor of 0.81 was computed for the longitudinal axis. The correction was applied to the response data rather than inserted in the simulation. The corrected responses and corresponding error functions are included in Fig. 12. GenHel validation was previously considered in Ref. 8 where an end-to-end time delay difference from flight data of 50 msec was computed, which is consistent with the present results. Some further comparisons with available flight data at several points in the control system were made and these indicated that the time delays are partly due to inaccuracies in the control system model and the remainder to inaccuracies in the rotor model. The servo actuator dynamic models have been verified so that the control portion of the delay is likely due to unmodeled linkage and mixer effects. The rotor portion of the delay is likely due to the lack of in-plane (lead-lag) structural flexing of the blades.³⁴ All remaining results in this paper will include the correction.

Handling qualities parameter results are collected in Fig. 13 for airspeeds of {0, 30, 50, 80} kt. Values vary little over the airspeed range considered, and GenHel essentially reproduces the flight test results, with ratings well inside the level 1 boundary for the lateral axis, and close to the boundary for the longitudinal axis. The lateral axis bandwidth is set by the frequency for 6 dB gain margin at all test speeds. Since this depends on the frequency for 180 deg phase shift, it is affected by the correction function. The longitudinal axis bandwidth was set by the 135 deg phase shift frequency, and this was less sensitive to the correction function.

Stability Margins. The SAS servo output sums with the pilot input as modeled in Fig. 14 to generate the mixer input. Flight data are available from sensors measuring the pilot stick deflection, δ_{PILOT} [AITD1], the mixer input, δ_{MX} , and the SAS servo output, δ_{SAS} , but not the linkage output, δ_f . Stability margins are defined from the “broken loop” control response, $\delta_f(s)/\delta_{MX}(s)$, but are often evaluated from the SAS servo and mixer sensor signals (FR_1 in Fig. 14). However, δ_f can be constructed indirectly as the difference between the mixer input and pilot signals and the stability margins computed from the indirect response (FR_2 in Fig. 14). The simulation represents the summing linkage as a simple gain which has been confirmed from low-frequency data, and the simulation gives identical responses by either method. The flight data, however, do not, as seen in Fig. 15. The differences are large at higher frequencies around the 180 deg phase shift frequency and this results in large differences in the computed gain margin. The response difference suggests unmodeled high-frequency losses in the SAS summing linkage. We consider the difference signal

(indirect method) as the more realistic one for computing stability margins since it measures the actual feedback to the rotor. In that case, gain margins cannot be predicted accurately without improvement to the linkage simulation model, but phase margins can be obtained since these depend on response behavior at lower frequencies where the two responses are much closer.

Stability margin results are shown in Fig. 16 for all test speeds. Gain margins are significantly higher from the indirect computation for both axes. Simulation gain margins match flight values from the direct method, which neglects the summing linkage dynamics and nonlinearities. These GM values are always less than the flight results from the indirect (exact) method so that the simulation yields conservative estimates. Phase margins from both methods and from the simulation agree well. The indirect computation of stability margins will be used hereafter.

4K Lb Block Load

Handling Qualities Parameters. Flight and simulation attitude responses, and the no-load response are compared in Fig. 17 for the lateral axis. For the lateral axis, the load introduces a gain dip and phase shift in the region of the pendulum mode frequency at about 1.6 rad/sec compared to the response without a load. In this region, the control inputs go into exciting the pendulum mode and less into exciting the helicopter, and there is a corresponding dip in the coherence. The load also causes the magnitude plot to flatten between the pendulum frequency and about 4 rad/sec while the no-load magnitude has a 20 dB/decade decline characteristic of rigid body dynamics. Gain and phase differences between flight and simulation in the frequency range 6–11 rad/sec are visible and suggest some excitation of rotor dynamics by the load not captured by the simulation. The corresponding error function (not shown) is close to the limit of the level D accuracy criteria in this range but there is nevertheless good agreement in bandwidth. A similar plot for the longitudinal axis (Fig. 18) shows much less effect of the load on the pitch attitude response.

One result of the gain dip in the lateral axis response is that there are multiple values for the 6 dB gain margin bandwidth, one of which is just below the pendulum frequency. A similar effect is found at all test airspeeds. The question arises as to whether pilot opinion of handling qualities is correlated with either of these bandwidths. Recent unpublished Army simulation trials at Ames suggest that neither of these suffices to predict pilot opinion, and the matter of what parameter predicts pilot opinion for the slung-load system remains an open

question. Lateral axis results for all test airspeeds are collected in Fig. 19. The simulation captures the multiple bandwidths and accurately predicts both bandwidth and phase delay in all cases, except that the lower bandwidth is not captured by the simulation at 80 kt owing to small differences in response magnitude around the pendulum frequency. As with the no-load case, the lateral axis bandwidth is determined by the 6 dB gain margin frequency at all test speeds. Results for longitudinal axis handling qualities parameters are collected in Fig. 20. In all cases, the 135 deg phase shift frequency determines bandwidth.

Stability Margins. The comparison of flight and simulation results in Fig. 21 for the test airspeeds, {0, 30, 50, 80} kt shows good agreement.

Pendulum Roots. The load on-axis angular rate frequency response plots for flight and simulation are compared in Fig. 22 for hover. The simulation is seen to reproduce the flight response closely. Lateral axis coherence is good over the frequency range shown and this was the case at all test airspeeds. Longitudinal axis coherence was poorer than the lateral axis at all test speeds, including a dip below 0.6 around the pendulum frequency. The loss in coherence in the region of the gain peak suggests the presence of nonlinearities in the response. While these are not yet understood, it is noted that the simulation captures the effect.

The second-order pole fit to the flight data was done over the frequency range [0.5, 2.5] rps. For the lateral axis the cost of the fit was high, above 100 at all test speeds, reflecting more complexity in the frequency response than is captured by a second-order pole model as shown in Fig. 5. The good coherence of the flight data tends to confirm the mismatch. For the longitudinal axis, the cost of the fit was well below 100 and this reflects greater agreement between the second-order pole model and the flight data. Some small-order differences between the two responses occur, probably related to the lower coherence of the flight data, but the gross trends in gain and phase match those of a second-order pole.

Results for the longitudinal and lateral pendulum roots are collected in Fig. 23 for test airspeeds to 80 kt. Load flight data were not available above 50 kt. For both modes, the natural frequency is closely predicted by the simulation and is seen to be nearly invariant with airspeed, and virtually the same for both axes. Damping results show good agreement at hover but differences develop with airspeed. The longitudinal pendulum is lightly damped, below 0.1, and this is reflected in its persistence in the flight time histories after it is excited. The lateral

pendulum is more damped, by way of its greater coupling with the aircraft attitude dynamics, and it is observed to die out in only a few cycles in flight.

4K Lb CONEX Load

Handling Qualities Parameters. Results for the CONEX lateral axis (Fig. 24) are similar to those for the 4K lb block load. Lateral axis bandwidth is again determined by the 6 dB gain margin frequency, which is double valued. Good agreement between flight and simulation is obtained except for the bandwidth at hover. This arises from frequency response differences in the range of 6–11 rps previously noted for the block in Fig. 17, but which result in a larger difference in the 6 dB gain margin values and a corresponding significant bandwidth prediction error in this case. Except for the hover flight test bandwidth, parameter values are nearly independent of airspeed, nearly the same as for the block, and closely predicted by the simulation. There is no significant effect of the CONEX's aerodynamics on the handling qualities parameters.

Stability Margins. The comparison of flight and simulation results in Fig. 25 for all tests speeds {0, 30, 50, 60, 70} kt indicates good agreement for the lateral axis. For the longitudinal axis, the flight results have significantly higher gain margins than the simulation predicts owing to the effect of the SAS summing linkage model error noted earlier.

Load Pendulum Roots. As airspeed increases, it was increasingly difficult to get load response flight data with adequate coherence for a credible identification of the pendulum roots. Coherence was insufficient above 50 kt. One difficulty is the CONEX spin rate, which increases with airspeed and which degraded the available load measurements. The second-order pole fit to the flight data succeeded better than for the block, with cost below 100 in all cases.

The collected results in Fig. 26 include simulation values with and without the load static aerodynamics. The pendulum frequency is seen to be accurately predicted by the simulation. The result is insensitive to the load static aerodynamics, and nearly identical to the pendulum frequency of the block. The flight data show a moderate increase in lateral pendulum damping with airspeed, and the simulation predicts this if the load static aerodynamics are included. The value of damping in hover is unaffected by the rotor downwash on the load. The lateral pendulum damping of the CONEX is a little higher than for the block, presumably owing to differences in load-sling geometry details, and this increase is captured by the simulation.

Trends. The existence of trends with load weight and airspeed is considered in Fig. 27 for the lateral axis handling qualities parameters. The simulation data include some results for a 6K lb block. The flight data show little variation in either bandwidth or phase delay with airspeed or load weight, and general values of 4 rad/sec for bandwidth (using the higher of the two values for bandwidth for cases with a load) and 0.15 sec for phase delay. An exception is the moderate loss of bandwidth at hover due to the load, with a different loss depending on the load. There is also a moderate increase in phase delay at [30, 50] kt for the test loads. The simulation results also show little variation with airspeed and load weight, and good general agreement with the flight values for these parameters. However, the simulation did not capture the hover loss in bandwidth due to the load and shows a sizeable difference in bandwidth at 30 kt.

Trends for lateral axis stability margins are considered in Fig. 28. The flight results show a differentiation in gain margin among loads at hover but not at higher airspeeds. The data include a 9K lb test load result at hover from Ref.4, which is consistent with a trend of increasing gain margin loss with load weight at hover. The simulation does not capture this variation and generally yields low gain margins owing to the SAS linkage modeling error. Flight values of phase margin also show consistent losses due to the load, particularly at hover. The simulation results for phase margin also show losses for the 4K and 6K lb block loads, while there is little or no loss for the CONEX. The no-load result at 30 kt contradicts this trend but the value may be affected by marginal coherence for the simulation data at this case, which also produces an out-of-trend value for the gain margin. The CONEX computations were repeated without load aerodynamics and there was no change in the result, so the difference between results for the CONEX and the blocks is presumed due to differences in load-sling geometry between these loads. The gain margin results for a 6K lb steel block are almost identical to the 4K lb block.

Conclusions

1. A slung-load simulation composed of the GenHel helicopter simulation model, the dynamic equations for the two-body slung load system and multi-cable sling, and load aerodynamics due to rotor downwash and static aerodynamics was implemented and compared with flight test data for the helicopter alone and for several test loads at airspeeds to 80 kt.
2. The fidelity of the GenHel helicopter simulation (no load) in producing the on-axis frequency responses for the longitudinal and lateral axes over the frequency range of interest in handling qualities work was evaluated. Important mismatches in the attitude response used to compute handling qualities parameters were noted in the region of 2 Hz due to control linkage and rotor dynamic modeling inaccuracies. These mismatches could be corrected empirically to obtain satisfactory agreement between simulation and flight data in attitude responses and in the handling qualities parameter values. Additional differences at higher frequencies were noted in the control responses used to evaluate stability margins which are likely due to a deficient model of the SAS linkage. These differences result in underestimated gain margins by the simulation. These results indicate that improvements to the GenHel control and rotor models would be useful in behalf of handling qualities and stability evaluations.
3. Good agreement was obtained between flight and simulation for the 4K lb block load which had negligible aerodynamics. The simulation was able to reproduce the effects of the load on the attitude, control loop, and load angular rate frequency responses underlying the dynamic parameters of interest, and to achieve good agreement in parameter values. The simulation reproduced such details as the multiple values of the lateral axis bandwidth, and differences between the longitudinal and lateral pendulum damping.
4. Good agreement was also obtained for the CONEX container, which has significant aerodynamics. The effect of load aerodynamics on pendulum damping was obtained for airspeeds short of instability. It was found that rotor downwash had no effect on the pendulum roots, while load static aerodynamics affected damping.
5. The simulation showed good overall agreement with flight values of all the parameters for the test points, and captured the effects of the loads, except for gain margin predictions. The use of this simulation for accurate prediction of the effect of load on stability margins requires more accurate modeling of the SAS linkage dynamics. However, the results obtained from the current model provide conservative estimates.
6. The GenHel UH-60 slung-load model, with corrections to account for some important secondary differences from flight, can be used for realistic analysis to evaluate handling qualities and stability, to develop control systems, to optimize load-sling configuration parameters, and as a basis for training or research simulators.

References

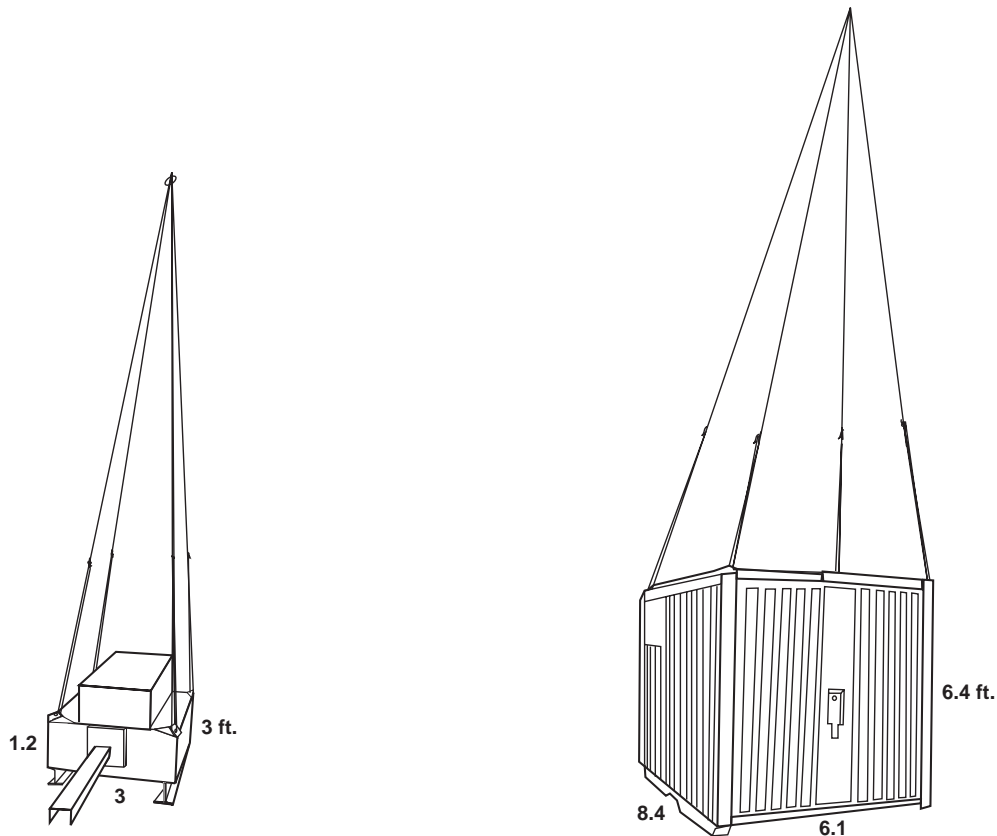
- ¹Negrette, A., Slingloads and Arrows. Rotor and Wing, Feb. 1999, p. 99.
- ²Conway, G. A., *Epidemiology and Prevention of Helicopter Logging Injuries*. Helicopter Logging Safety. National Institute for Occupational Safety and Health. M. L. Klatt, ed., July 1998.
- ³Multiservice Helicopter External Air Transport; Vols. I, II, III. U.S. Army FM-55-450-3, 4, 5, Feb. 1991.
- ⁴Lawrence, T., Gerdes, W., Yakzan, S., Use of Simulation for Qualification of Helicopter External Loads. Proceedings, AHS Forum, May 1994.
- ⁵McCoy, A. H., Flight Testing and Real Time System Identification Analysis of a UH-60A Black Hawk Helicopter with an Instrumented External Sling Load. NASA CR 1998-196710, April 1998.
- ⁶Cicolani, L. S., McCoy, A. H., Tischler, M. B., Tucker, G. E., Gatenio, P., Marmar, D., Flight Time Identification of a UH-60A Helicopter and Slung Load. NASA TM 1998-112231, April 1998.
- ⁷Howlett, J. J., UH-60A Black Hawk Engineering Simulation Program: Math Model and Background Report. NASA CR 166309 and 166210, Dec. 1981.
- ⁸Ballin, M. G., Dalang-Secretan, M., Validation of the Dynamic Response of a Blade-element UH-60 Simulation Model in Hovering Flight. Proceedings, AHS Forum, May 1990.
- ⁹Ballin, M. G., Validation of a Real-Time Engineering Simulation of the UH-60A Helicopter, NASA TM 88360, Feb. 1987.
- ¹⁰Rosen, A., Yaffe, R., Mansur, M. H., Tischler, M. B., Methods for Improving the Modeling of Rotor Aerodynamics for Flight Mechanics Purposes. Proceedings, AHS Forum, 1998.
- ¹¹Ten Years of Cooperation on Rotorcraft Aeromechanics and Man-Machine Integration Technology. M. B. Tischler, A. Kuritsky, eds., Ames Research Center, Oct. 1996.
- ¹²Kufeld, R., Balough, D., Cross, J., Stuebaker, K., Jennison, C., Bousman, W., Flight Testing the UH-60A Airloads Aircraft. Proceedings, AHS Forum, May 1994.
- ¹³Hilbert, K., A Mathematical Model of the UH-60 Helicopter. NASA TM 85890, April 1984.
- ¹⁴Williams, J. M., Ham, J. A., Tischler, M. B., Flight Test Manual: Rotorcraft Frequency Domain Flight Testing. AQTD Project 93-14, U.S. Army Aviation Technical Test Center, Sept. 1995.
- ¹⁵Tischler, M. B., Cauffman, B., Frequency-Response Method for Rotorcraft Identification: Flight Applications to BO-105 Coupled Rotor/Fuselage Dynamics. JAHS, Vol. 37, No. 3, July 1992.
- ¹⁶Tischler, M. B., System Identification Methods for Aircraft Flight Control Development and Validation, NASA TM 110369, Oct. 1995.
- ¹⁷Handling Qualities Requirements for Military Rotorcraft, U.S. Army Aeronautical Design Standard ADS-33D-PRF, USAATC/AVRDEC, U.S. Army Aviation and Troop Command, St Louis, May 1996.
- ¹⁸MH-53J AFCS Evaluation. Project A-8867 Final Report. Georgia Tech Research Institute, Nov. 1993.
- ¹⁹Cicolani, L. S., Kanning, G., Equations of Motion of Slung-Load Systems, Including Multilift Systems. NASA TP 3280, Nov. 1992.
- ²⁰Cicolani, L. S., Kanning, G., Synnstedt, R., Simulation of the Dynamics of Helicopter Slung Load Systems. JAHS, Oct. 1995.
- ²¹Pitt, D. M., Peters, D. A., Theoretical Prediction of Dynamic Inflow Derivatives. Vertica, Vol. 5, 1981.
- ²²Ballin, M. G., A High-Fidelity Real-Time Simulation of a Small Turboshaft Engine. NASA TM-100991, 1988.
- ²³Bailey, F. J., A Simplified Theoretical Method of Determining the Characteristics of a Lifting Rotor in Forward Flight. NACA TR 716, 1941.
- ²⁴Ronen, T., Dynamics of a Helicopter with a Sling Load. Dept of Aeronautics and Astronautics, Stanford University, Palo Alto, CA, 1985.
- ²⁵McKee, J. W., Naeseth, R. L., Experimental Investigation of the Drag of Flat Plates and Cylinders in the Slipstream of a Hovering Rotor. NACA TN 4239, April 1958.
- ²⁶Boatwright, D. W., Measurements of Velocity Components in the Wake of a Full-Scale Helicopter Rotor in Hover. USAAMRDL TR-72-33, Fort Eustis, VA, Aug. 1972.
- ²⁷Laub, G. H., Kodani, H. M., Wind Tunnel Investigation of Aerodynamic Characteristics of Scale Models of Three Rectangular Cargo Containers. NASA TM X-62169, July 1972.
- ²⁸Laub, G. H., Kodani, H. M., Wind Tunnel Investigation of Aerodynamic Characteristics of a Scale Model of a D5 Bulldozer and an M109 Self-Propelled 155 mm Howitzer. NASA TM X-62330, Jan. 1974.
- ²⁹Sheldon, D. F., An Appreciation of the Dynamic Problems Associated with the External Transportation of Loads from a Helicopter—State of the Art. Vertica, Vol. 1, 1977.
- ³⁰Watkins, T. C., Sinacori, J. B., Kessler, D. F., Stabilization of Externally Slung Helicopter Loads. USAAMRDL TR-74-42, Aug. 1974.

³¹Simpson, A., Flower, J. W., Unsteady Aerodynamics of Oscillating Containers and Application to the Problem of Dynamic Stability of Helicopter Underslung Loads. AGARD-CP-235, May 1978.

³²Miller, D. G., Lu, Y., White, F., Osciak, E., Roberts, B., Price, R., Wiedorn, J., Flight Simulation as a Tool to Develop V-22 Slung Load Capabilities. Proceedings, AHS Forum, May 1999.

³³Mansur, M. H., Tischler, M. B., An Empirical Correction for Improving Off-Axes Response in Flight Mechanics Helicopter Models. JAHS, April 1998.

³⁴Curtiss, H. C.: On the Calculation of the Response of Helicopters to Control Inputs. 18th European Rotorcraft Forum, Avignon, France, Sept. 1992.



Load parameters

	4K Block	Ballasted Conex
Weight	3895	4105 lb
Density	365	12.5 lb/ft ³
Ixx	103	1876 slg-ft ²
Iyy	103	1482
Izz	174	1377

Aircraft parameters

Nominal takeoff weight	14601 lb
Max takeoff weight	22250 lb
Ixx, Iyy, Izz	5629, 40000, 37200 lb-ft ³
Hook capacity	8000 lb
Nominal cg-to-hook coordinates	(0.98, 0, 4.3) ft

Sling parameters (each leg)

Leg length	15.83 ft
Spring constant	9645 lb/ft
Spring damping	22 lb/ft/sec

Fig. 1 Test configurations and parameters.

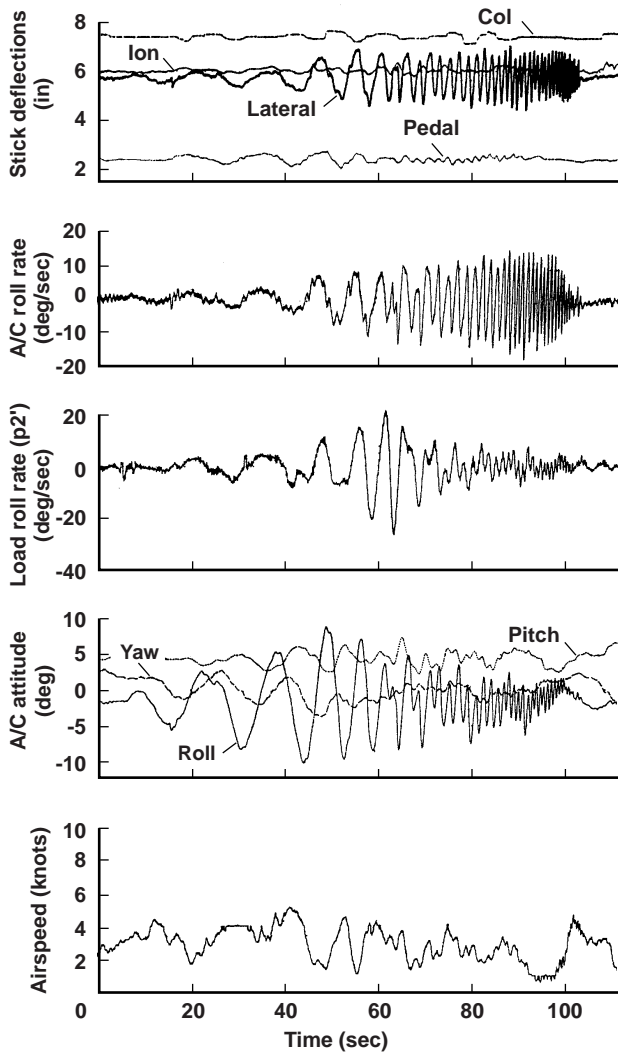
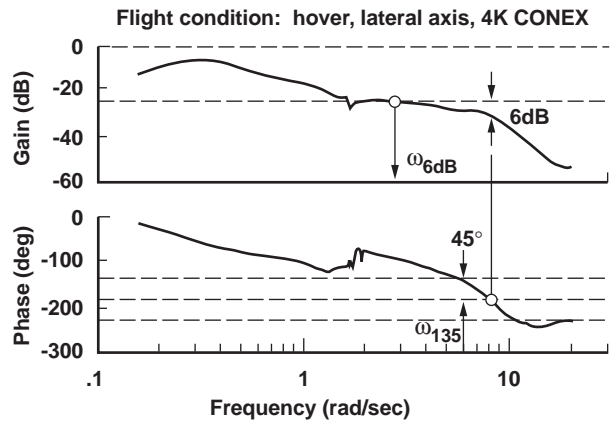


Fig. 2 Sample lateral frequency sweep.



Bandwidth: $\omega_{BW} = \min \{ \omega_{6dB}, \omega_{135} \}$

Phase delay: $\tau_{PD} = -\frac{\Phi(2\omega_{180}) + 180}{2\omega_{180}}$ or $-\frac{1}{2} \left(\frac{d\Phi}{d\omega} \right)_{\Phi = 180}$

ADS-33D HQ Ratings

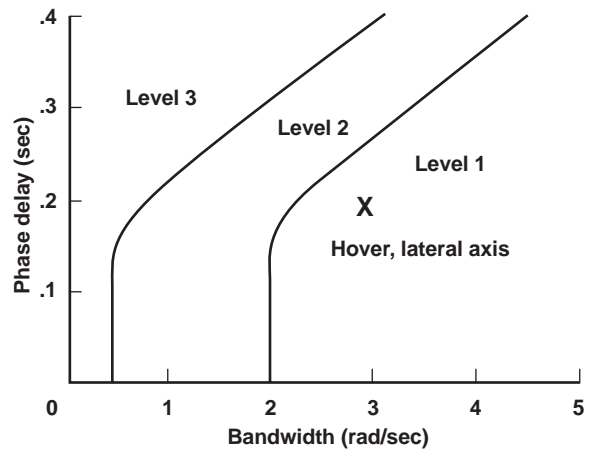


Fig. 3 Identification of handling qualities parameters from attitude response.

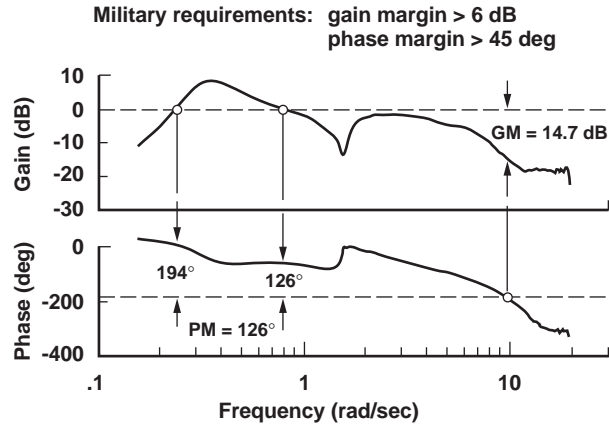


Fig. 4 Identification of stability margins from control response $\delta_{SAS}/\delta_{TOTAL}$.

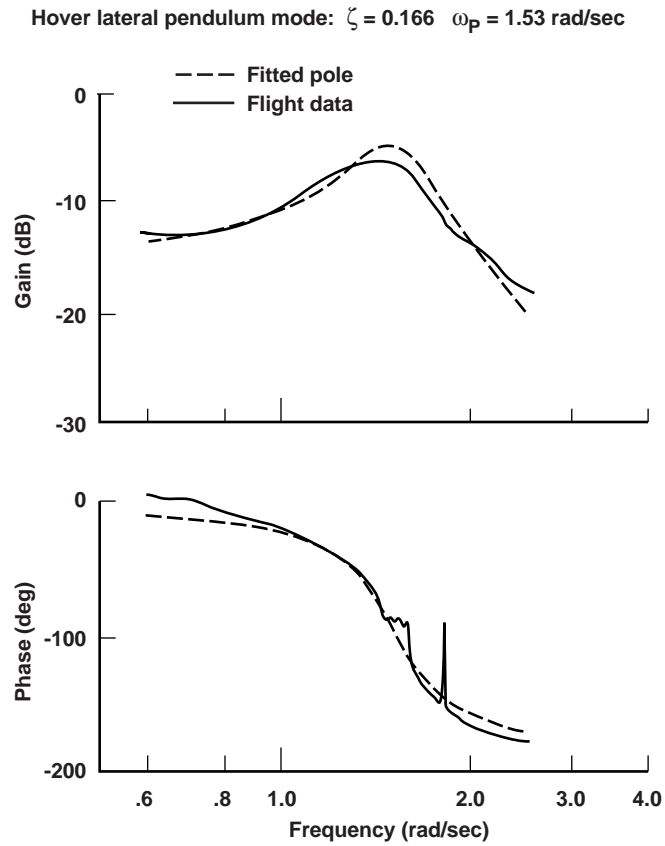


Fig. 5 Identification of load pendulum roots.

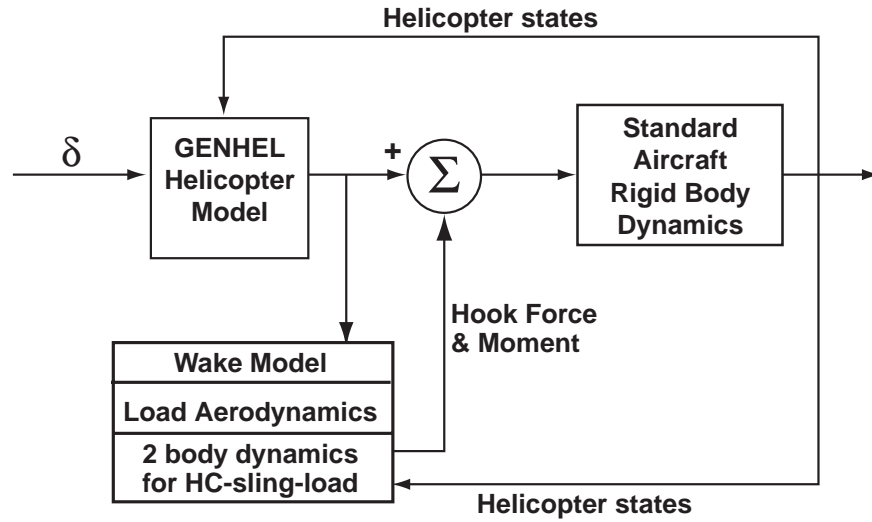


Fig. 6 Integration of slung load into standard helicopter simulation.

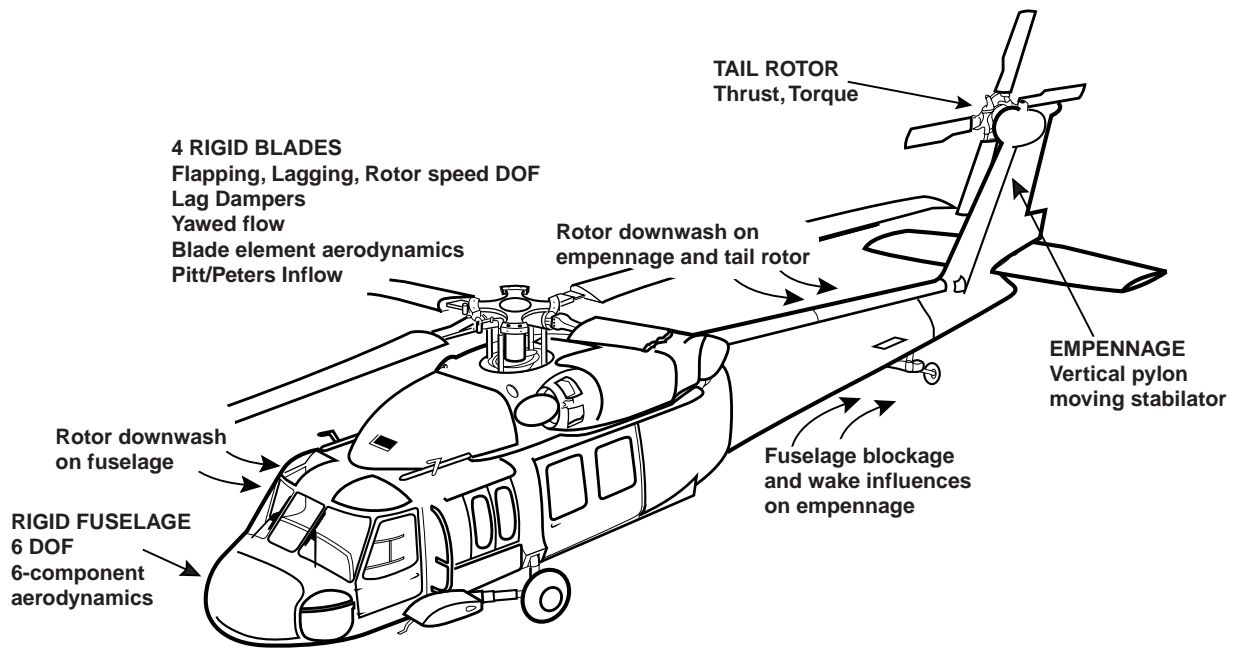


Fig. 7 Components of GenHel UH-60 simulation.

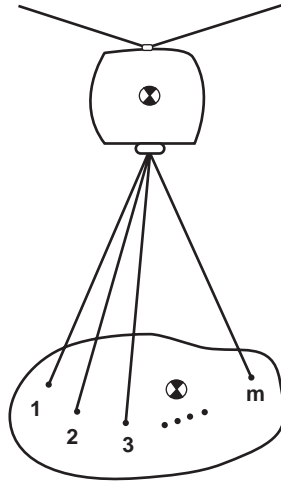


Fig. 8 Generic multi-cable sling configuration.

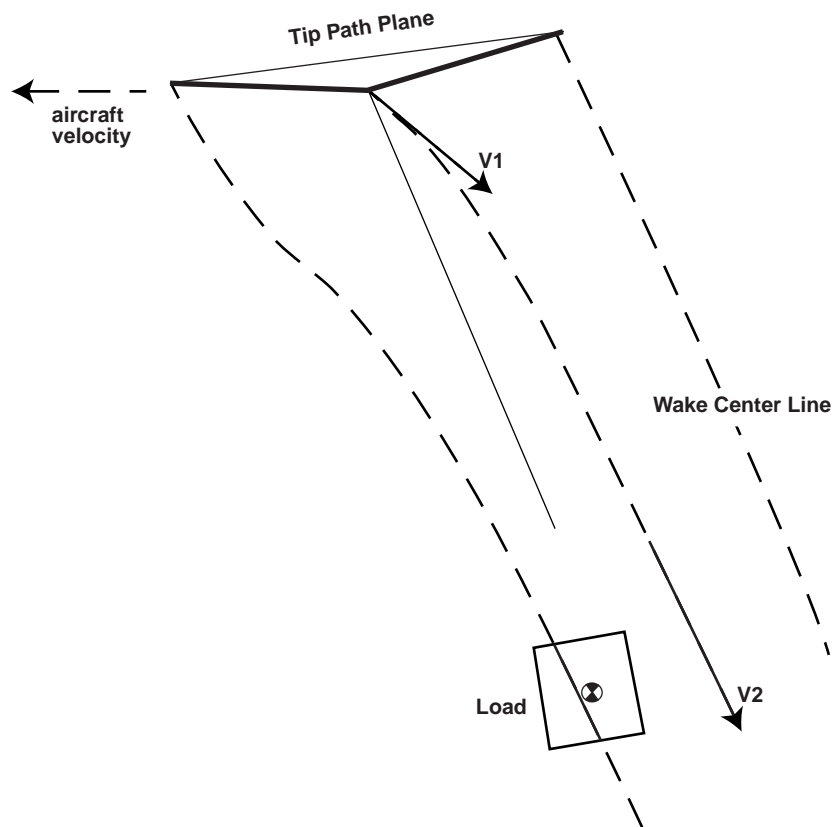
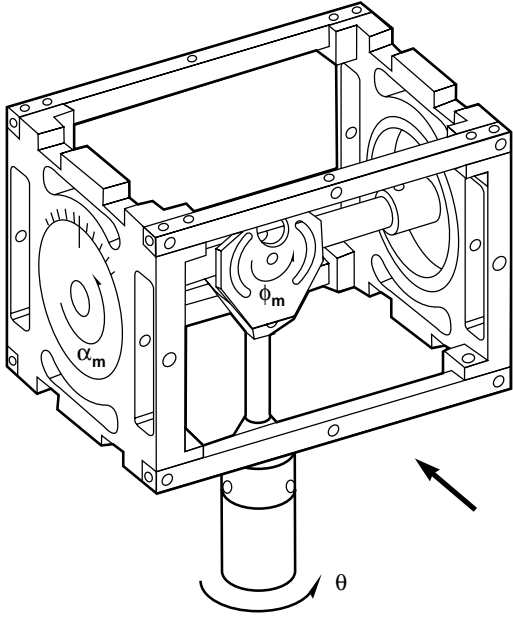
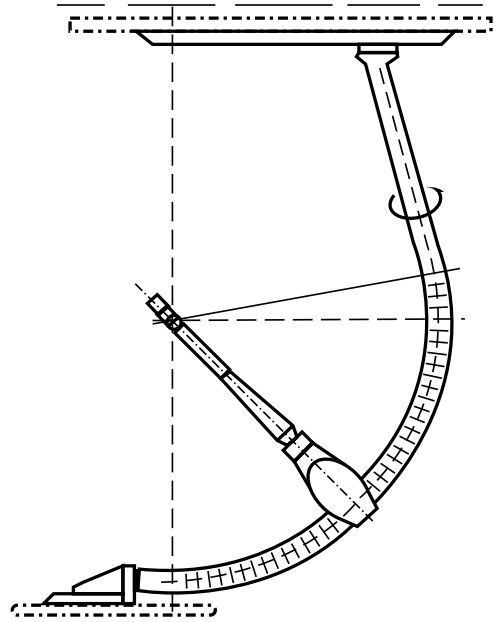


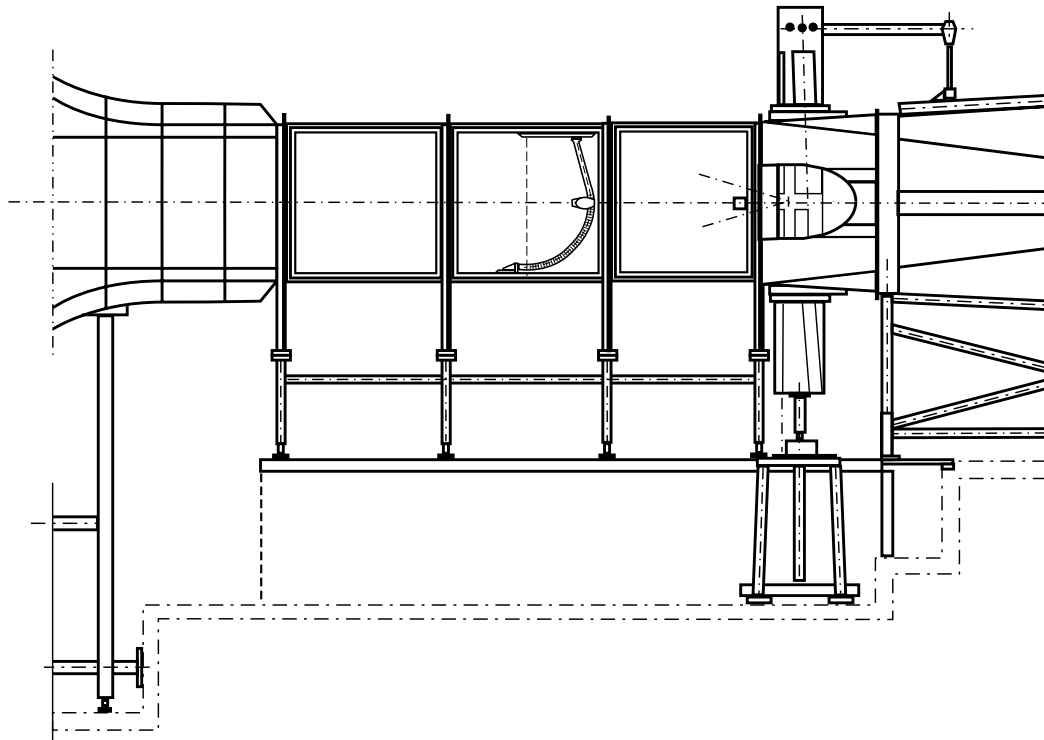
Fig. 9 Rotor wake geometry.



CONEX model internal mechanism



"Banana" arm model support



Tunnel

Fig. 10 Technion 1 × 1 m Low Speed Wind Tunnel.

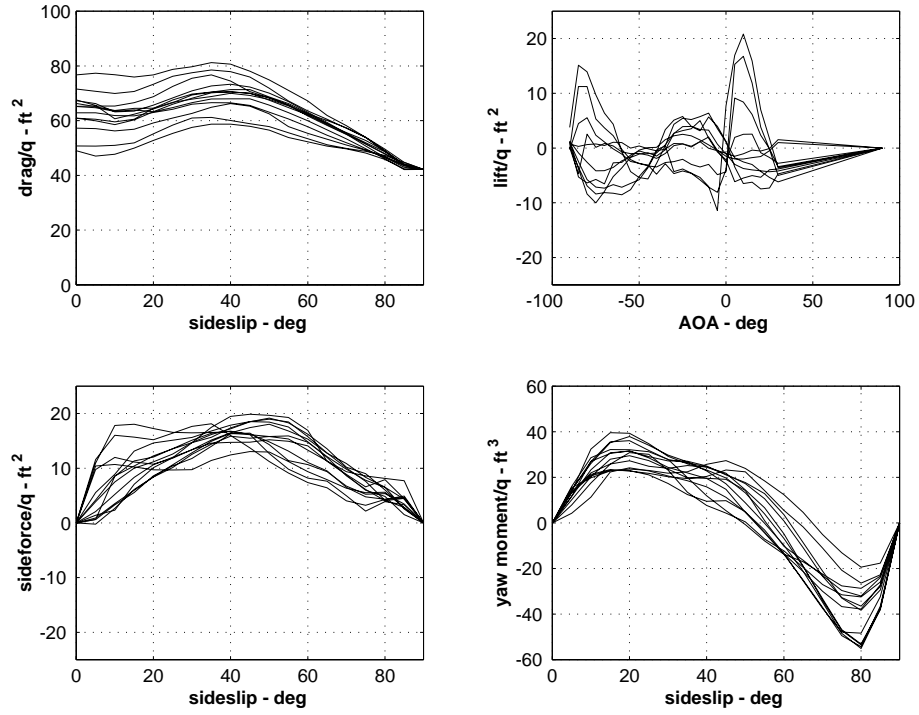


Fig. 11 CONEX static aerodynamics.

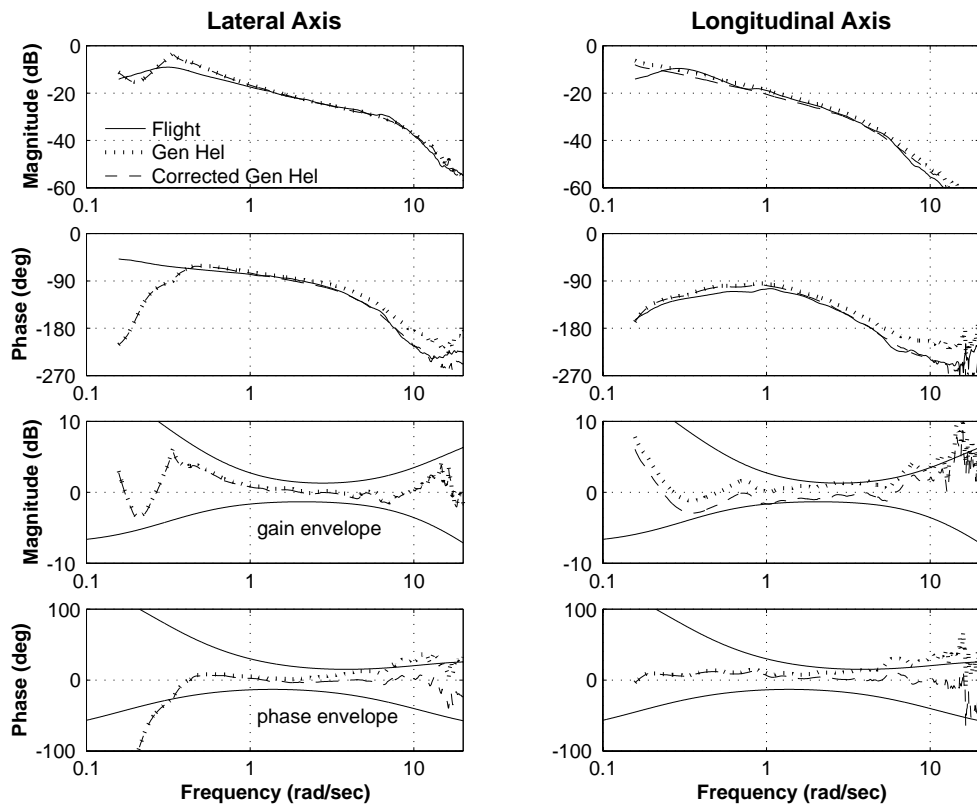


Fig. 12 Attitude response and error functions: no load.

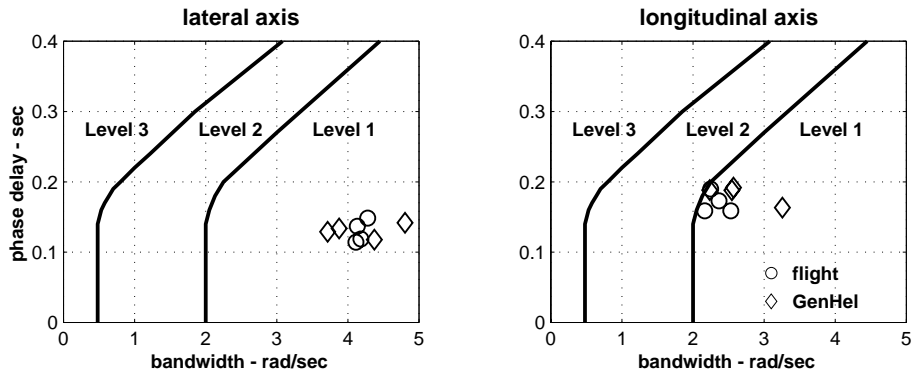


Fig. 13 Handling qualities parameters: no load.

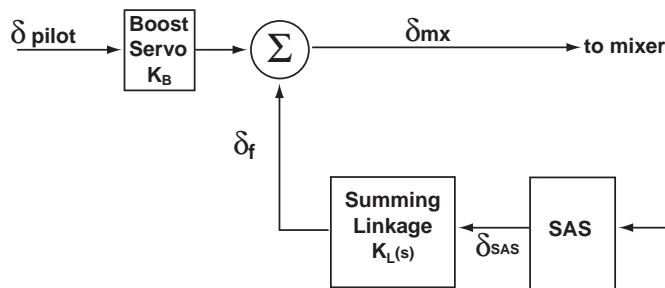


Fig. 14 Computation of stability margins.

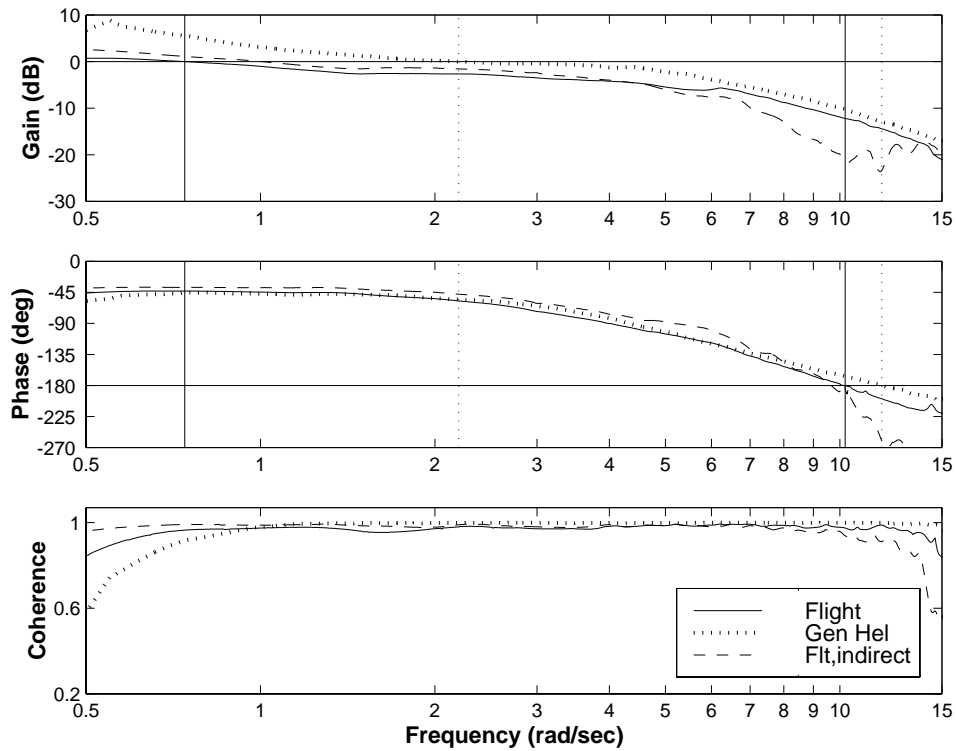


Fig. 15 Control response: no load, lateral axis, hover.

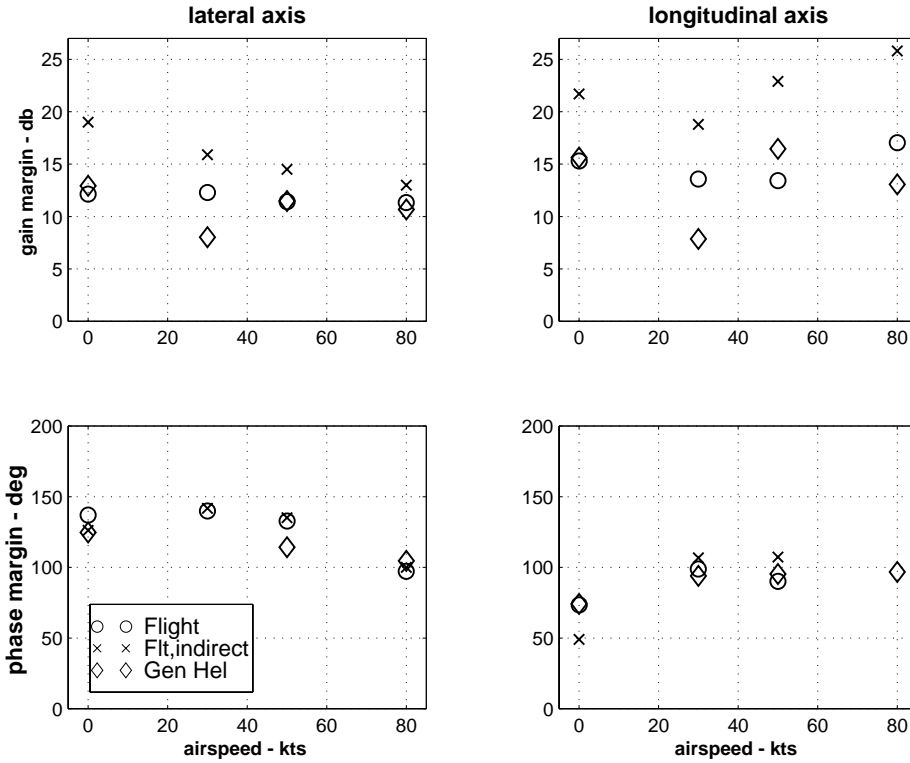


Fig. 16 Stability margins: no load.

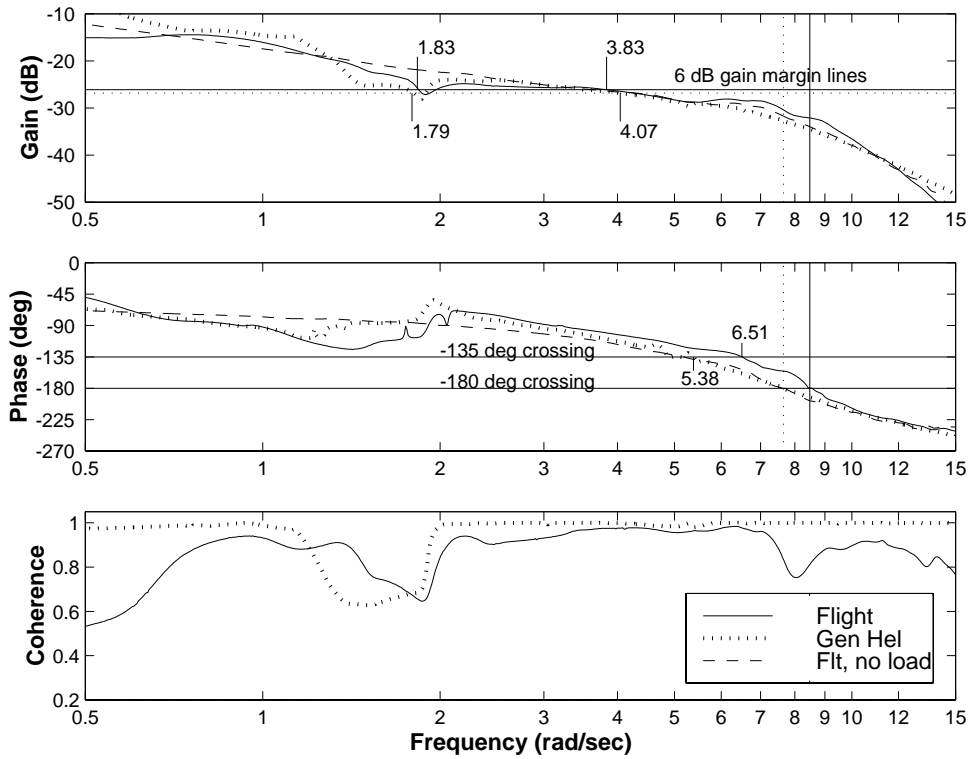


Fig. 17 Attitude response: 4K lb block load, lateral axis, hover.

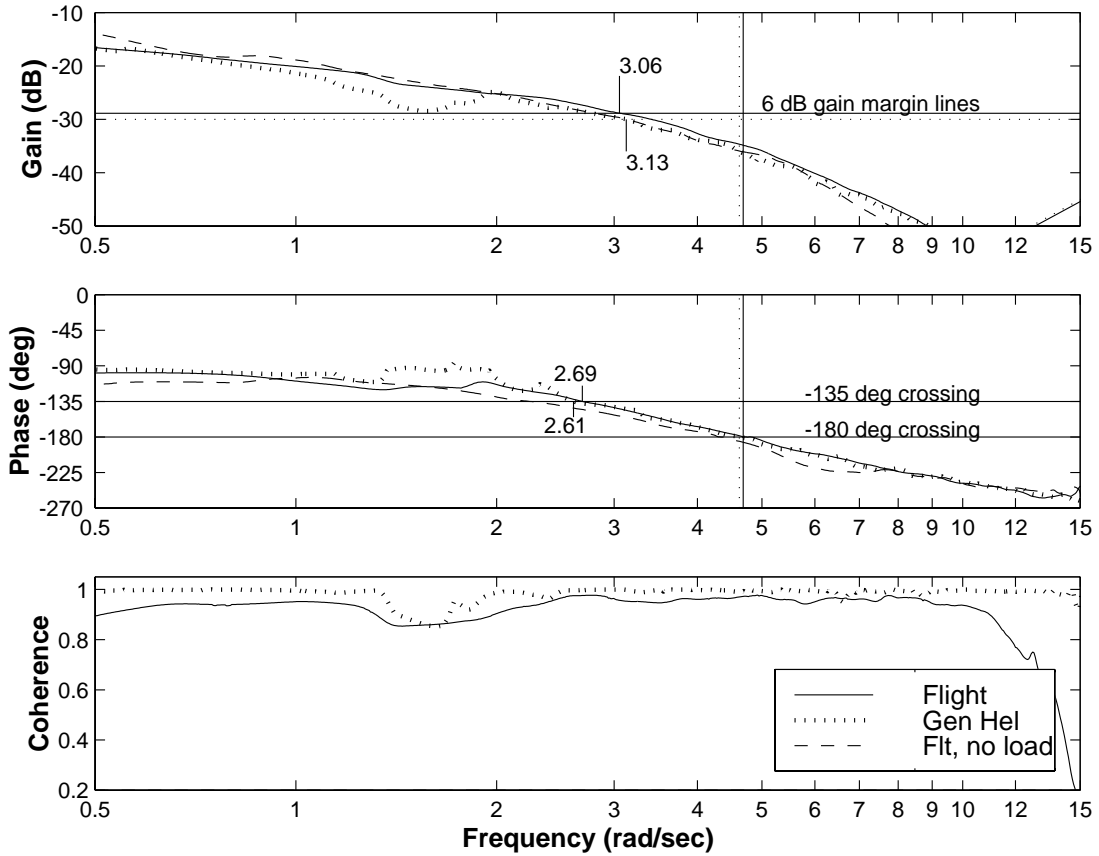


Fig. 18 Attitude response: 4K lb block load, longitudinal axis, hover.

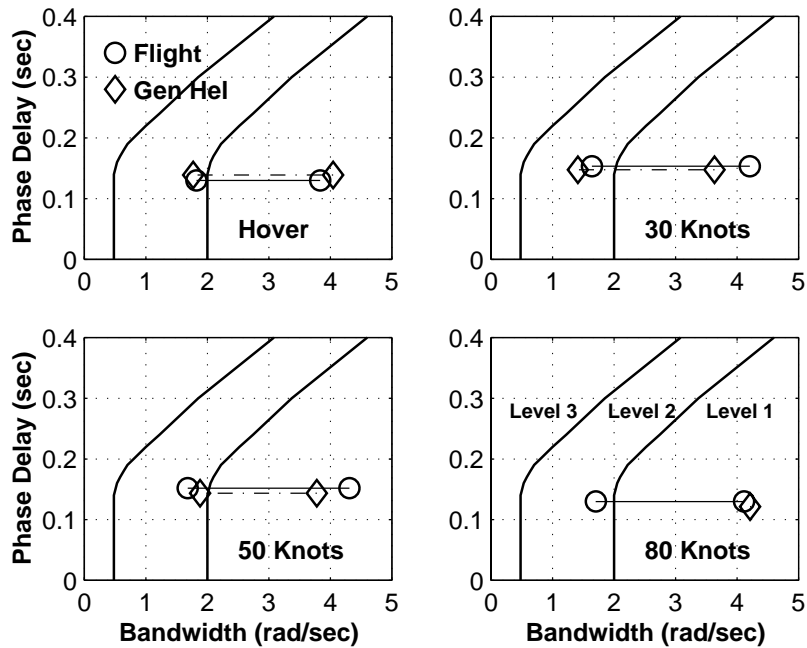


Fig. 19 Handling qualities parameters: 4K lb block load, lateral axis.

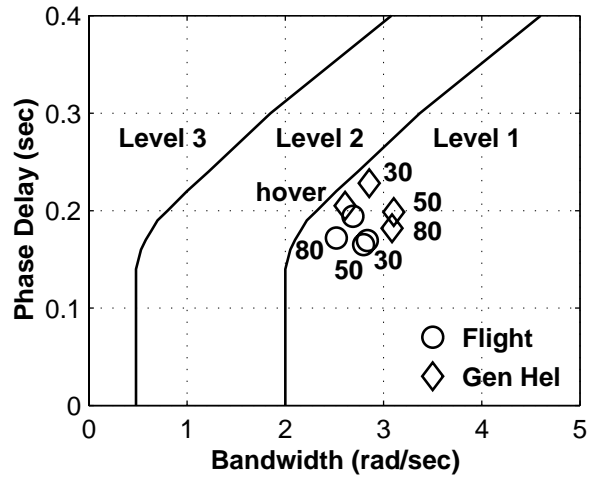


Fig. 20 Handling qualities parameters: 4K lb block load, longitudinal axis.

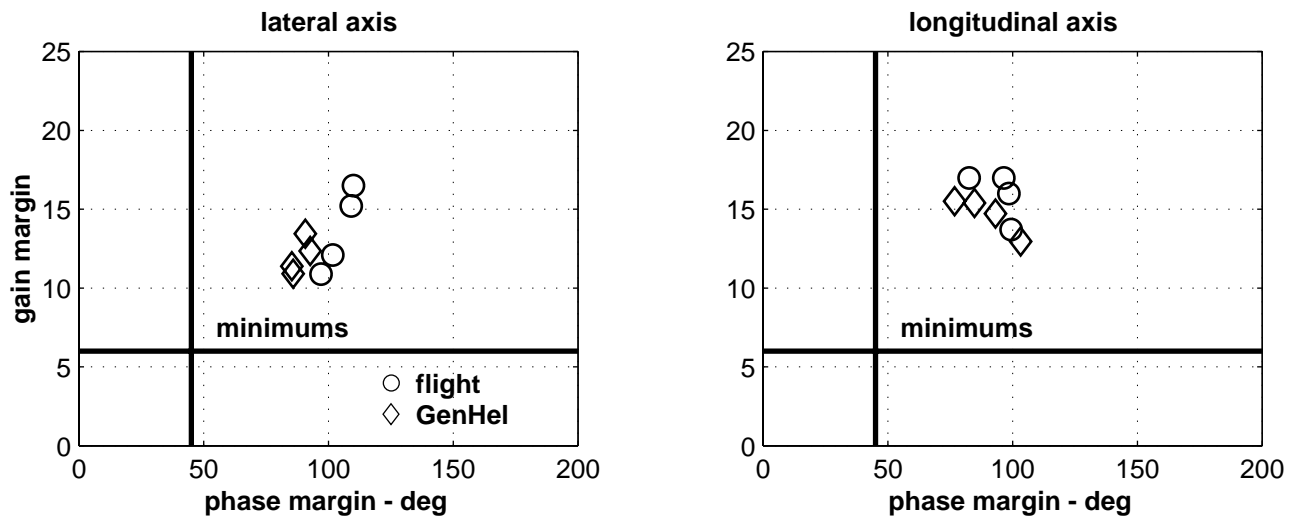


Fig. 21 Stability margins: 4K lb block load.

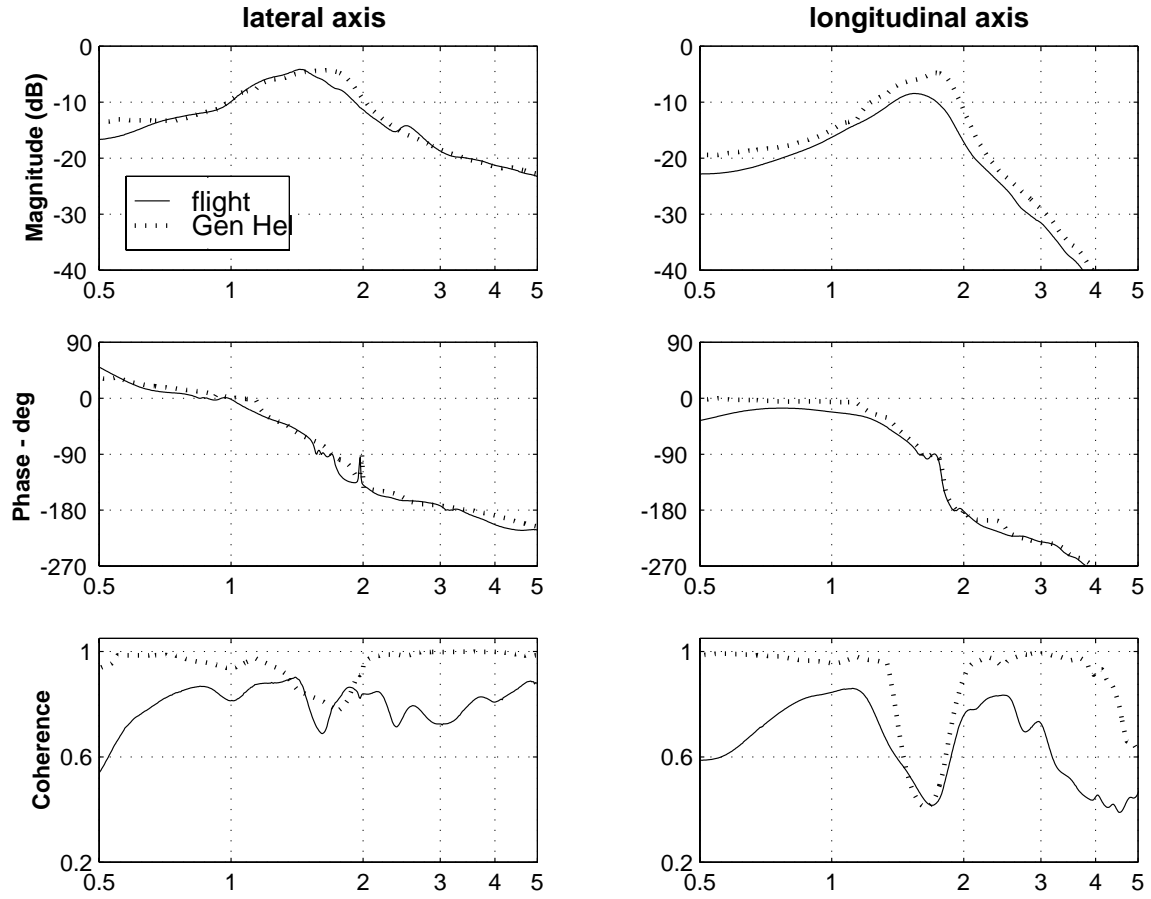


Fig. 22 Load angular rate response: 4K lb block load, hover.

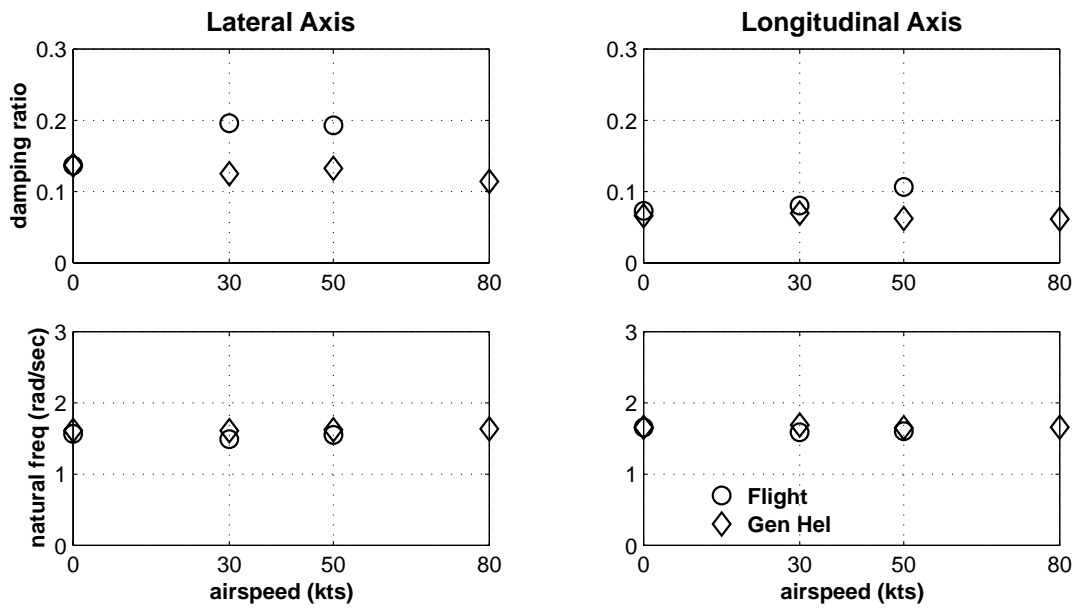


Fig. 23 Pendulum roots: 4K lb block load.

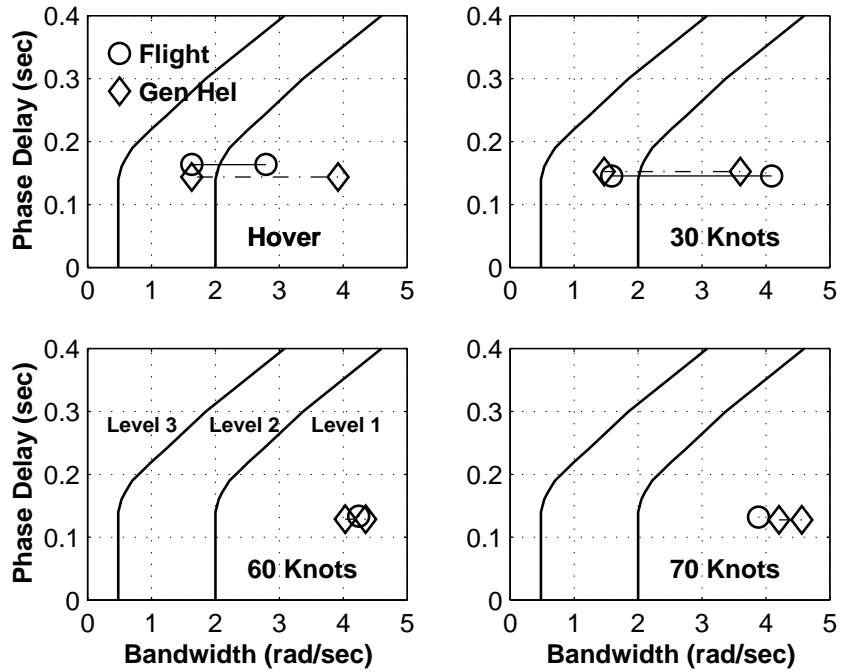


Fig. 24 Handling qualities parameters: CONEX load, lateral axis.

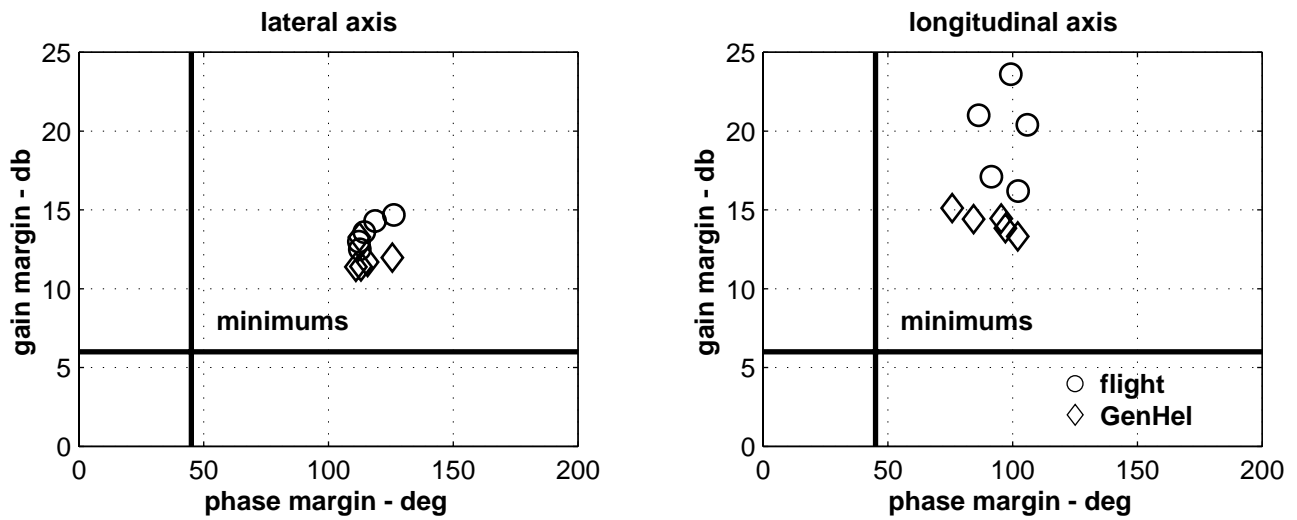


Fig. 25 Stability margins: CONEX load.

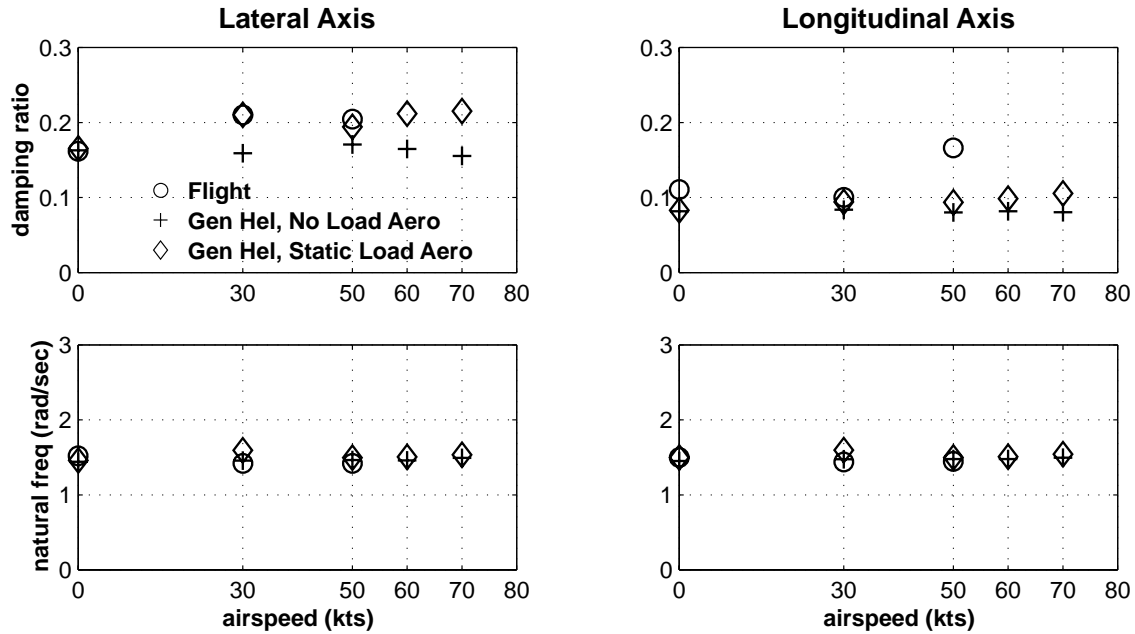


Fig. 26 Pendulum roots: CONEX load.

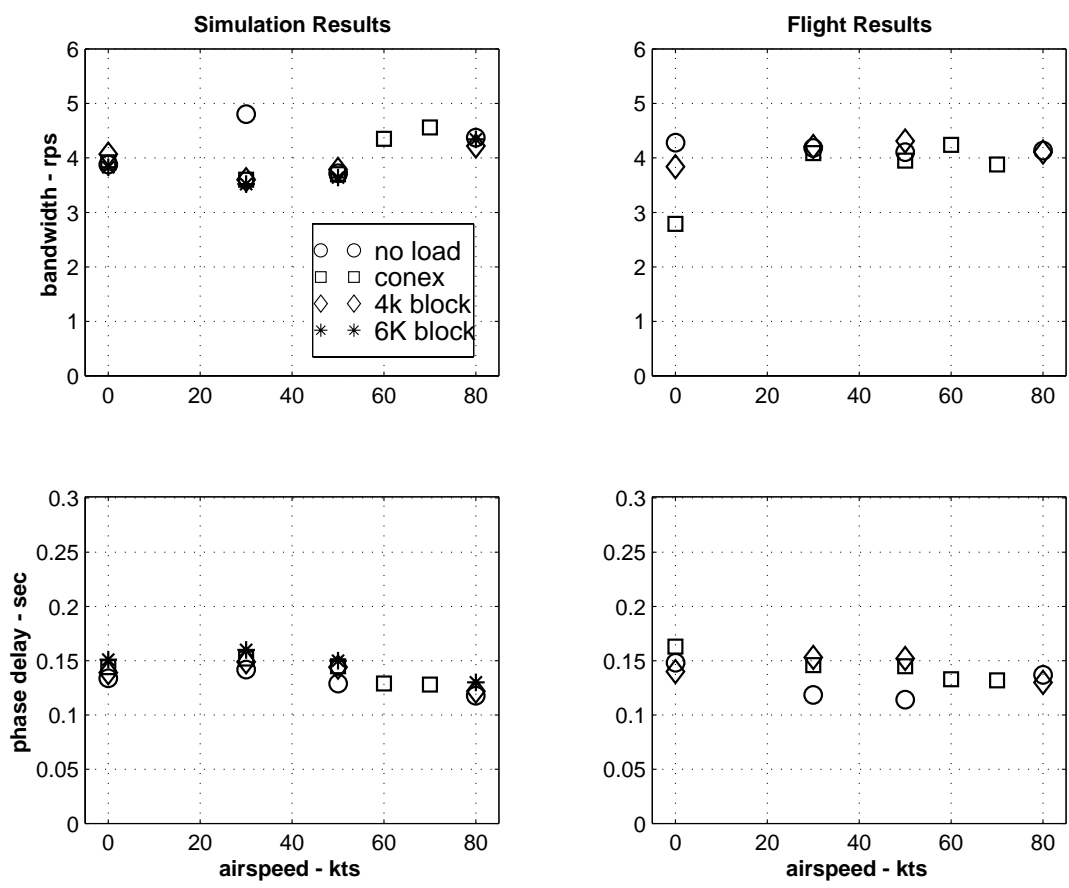


Fig. 27 Lateral axis handling qualities parameters: effect of airspeed and load weight.

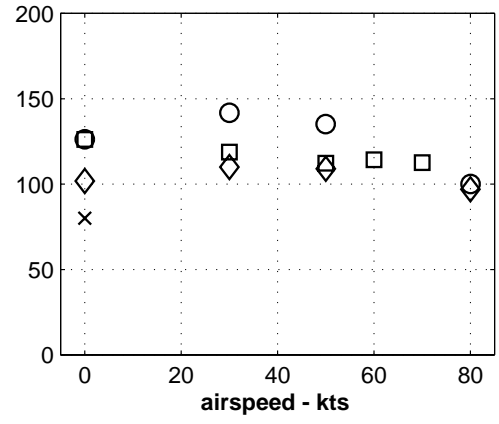
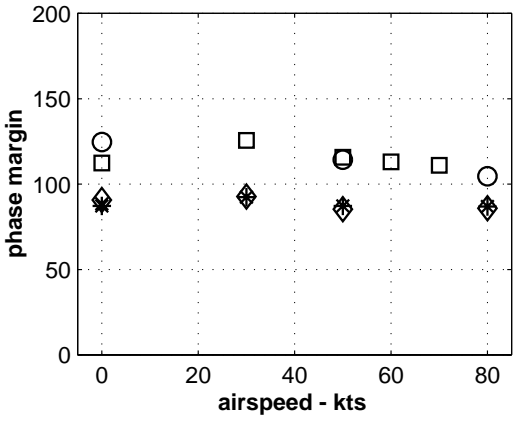
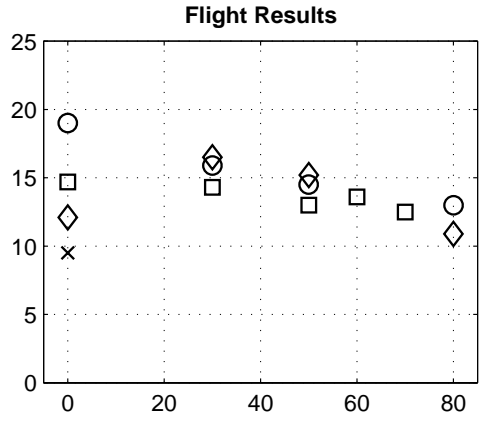
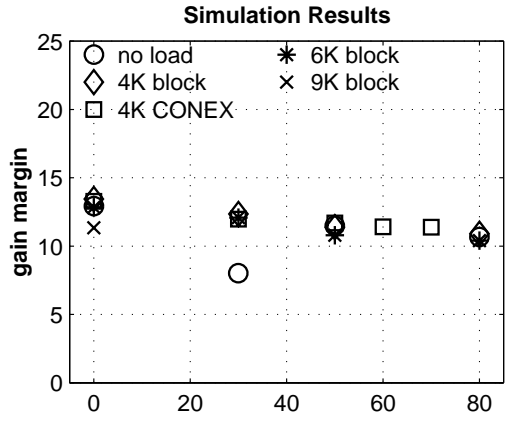


Fig. 28 Lateral axis stability margins: effects of airspeed and load weight.